ELSEVIER

Physica C 295 (1998) 177–185

PHYSICA C

Fast determination of 2D current patterns in flat conductors from measurement of their magnetic field

Rinke J. Wijngaarden *, K. Heeck, H.J.W. Spoelder, R. Surdeanu, R. Griessen

Department of Physics and Astronomy, Vrije Universiteit, De Boelelaan 1081, 1081 HV Amsterdam, Netherlands

Received 23 September 1997; accepted 17 October 1997

Abstract

An extremely fast method is presented to calculate the local current–density vector in a flat conductor from the z-component of the magnetic field measured above its surface, e.g. by means of magneto-optical indicators, Hall-probe arrays or scanning SQUIDs. The method may be used for samples of arbitrary thickness provided that the current vector has only x- and y-components. The method combines the conjugate gradient (CG) method and fast Fourier transform to invert the relevant Toeplitz matrix equation. For a current map of $n \times n$ pixels, the number of operations needed is of order $n^{2.8}$ only, compared to $n^{4.5}$ or higher for earlier methods. The increase in speed for 512×512 pixels is found to be a factor 135 with respect to the fastest existing CG method. © 1998 Elsevier Science B.V.

Keywords: Superconductivity; Magneto-optics; Biomagnetic inversion

1. Introduction

In this paper we discuss an imaging technique which yields a map of current flowing in a sample provided that this current flow is two dimensional. Current flow imaging has biomedical applications [1–3] for the contact free measurement of e.g. current flowing in neurons, in which case the magnetic field is detected using e.g. a SQUID magnetometer. It is also widely applied to detect the current flow in flat superconducting samples [4–6], where the local magnetic field is often detected using the Faraday effect in magneto-optical indicators [7]. The experimental current flow can be compared with a wealth of theoretical predictions [8–13].

Here we focus on the use of the magneto-optical detection technique in the field of superconductivity. Since the relevant experimental details were extensively discussed in a previous paper [4], we give a short summary only. It is required that the current flow is two-dimensional: to be specific we assume that the z-component of the current vector is zero and that within the sample of arbitrary thickness t, the current vector is independent of z (see Fig. 1 for the sample configuration). In that case the current–density map $\vec{j}(\vec{s}) = \vec{j}(x,y)$ can be reconstructed from the measured $H_z(x,y)$-field using an algorithm which essentially inverts the Biot–Savart law. Due to the highly non-local relation between current and magnetic field such inversion is far from trivial. The various methods proposed so far fall broadly into two categories: (i) slow accurate real-space methods and (ii) fast methods in Fourier space which lead

* Corresponding author. Tel.: +31 20 444 7918; Fax: +31 20 444 7899; E-mail: rw@nat.vu.nl

0921-4534/98/$19.00 © 1998 Elsevier Science B.V. All rights reserved.
PII S0921-4534(97)01799-1

inherently to inaccuracies. In our previous work [4] we succeeded in reducing the number of operations for the slow real space method from $O(n^6)$ to $O(n^{4.5})$ for the case of a current map containing $n \times n$ pixels. In this work the real space method is improved to such extent that the number of operations is drastically lowered further to $O(n^{2.8})$. This leads to a reduction in inversion time of typically two orders of magnitude. This is a milestone on the way to real-time applications.

After a summary of the electro-magnetic problem the various known methods will be discussed, then the new method will be presented.

2. The electromagnetic inversion problem

Consider a sample (see Fig. 1) with a two dimensional current flow pattern $\vec{j}(\vec{s})$ as defined above. The field $\vec{H}$ at any position $\vec{r}$ generated by these currents is given by the Biot–Savart equation [14]:

$$\vec{H}(\vec{r}) = \frac{1}{4\pi}\int_V \vec{j}(\vec{s}) \times \frac{\vec{r}-\vec{s}}{|\vec{r}-\vec{s}|^3}\,\mathrm{d}^3 s, \tag{1}$$

where the integral is over the volume of the sample V. Since currents are not flowing outside the sample, the integral can also be taken over the whole space. For a 2D-current pattern, where the currents are flowing parallel to the (xy)-plane, Brandt [15] introduced the scalar field g, defined by:

$$\vec{j}(\vec{s}) \equiv \nabla_{\vec{s}} \times \left[g(\vec{s})\,\hat{z} \right], \tag{2}$$

which guarantees that $\nabla \cdot \vec{j} = 0$. In fact, g is defined apart from an integration constant and a gradient term, which both are chosen to be zero. Note that contrary to Brandt [15] we do not use the concept of sheet currents, hence in the present work the integral in Eq. (1) is also over the thickness t of the sample, while the dimension of j is $\mathrm{A/m^2}$, and of g is $\mathrm{A/m}$.

The measurement is typically discrete (e.g. due to the pixels of the CCD camera in the magneto-optical experiment): the field H_z is measured on a rectangular grid of unit cell a (labelled 'detector' in Fig. 1 and hereafter called the H_z-image) which is parallel to the sample and at a distance d from the closest (flat) surface of the sample. We calculate g on a similar grid containing the surface of the sample (hereafter called the g image). Using this spatial discretization, the following equation is found [4] for the component of the field along z:

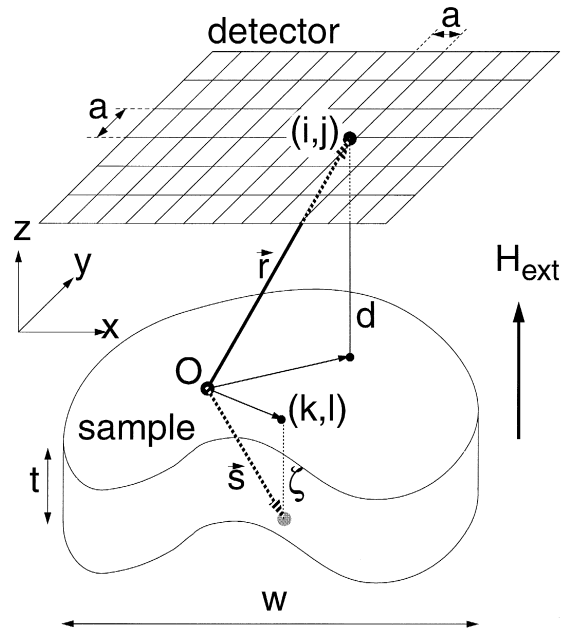

Fig. 1. Schematic representation of the experimental lay-out. The measurement of the H_z-field is done in the detector plane with a spatial resolution corresponding to pixels of size $a \times a$. The sample thickness is t and the distance of observation is d. The other symbols are explained in the text.

$$H_z(i,j;a,d,t) = \frac{1}{4\pi}\sum_{k,l} g(k,l) \int_{k+\frac{1}{2}}^{k-\frac{1}{2}} \int_{l+\frac{1}{2}}^{l-\frac{1}{2}} \int_t^0 \frac{2(d+\zeta)^2 - a^2(\xi-i)^2 - a^2(\eta-j)^2}{\left[(d+\zeta)^2 + a^2(\xi-i)^2 + a^2(\eta-j)^2\right]^{5/2}} \times a^2\,\mathrm{d}\zeta\,\mathrm{d}\eta\,\mathrm{d}\xi, \tag{3}$$

where ξ, η and ζ are along x, y and z, respectively. The (integer) pixel coordinates are (k,l) in the g-image and (i,j) in the H_z-image. Eq. (3) can be written as:

$$H_z(i,j) = \frac{1}{4\pi}\sum_{k,l} M(i,j,k,l)\,g(k,l), \tag{4}$$

where $M(i,j,k,l)$ is the integral in Eq. (3). Although not explicitly written, $H_z(i,j)$ and $M(i,j,k,l)$ depend on the pixel size a, the sample thickness t and the distance d between the H_z image and the sample surface. Note that if H_z is measured at $n \times n$ positions, $M(i,j,k,l)$ has n^4 elements; typically $n = 512$ and $n^4 \simeq 7 \times 10^{10}$.

The matrix M is in fact a four dimensional Toeplitz matrix since:

$$M(i,j,k,l) = \tilde{m}(|i-k|,|j-l|) = :m(i-k,j-l), \quad (5)$$

where the last equality defines a matrix m to be used below. The property $M(i,j,k,l) = \tilde{m}(i-k,\ j-l)$ was used in Ref. [4] to reduce the amount of required storage from $O(n^4)$ to $O(n^2)$.

3. Fourier transform methods

Fourier transform (FT) methods exploit the fact that Eq. (4) represents a convolution: if Eq. (5) is taken into account one may write: $4\pi H_z = m \otimes g$ (the convolution is indicated by $\otimes$) hence $\mathrm{FFT}(4\pi H_z) = \mathrm{FFT}(m) \times \mathrm{FFT}(g)$. The scalar field g is thus efficiently calculated from

$$g = \mathrm{IFFT}\left[\frac{\mathrm{FFT}(4\pi H_z)}{\mathrm{FFT}(m)}\right], \quad (6)$$

where IFFT and FFT denote the (inverse) fast Fourier transform. Analytic Fourier transform applied to the analytic equations or FFT applied to the discretized ones shown above are e.g. at the basis of the work of Roth et al. [16] and Johansen et al. [17].

Unfortunately FT-methods have several drawbacks. (i) For large k-vectors $\mathrm{FFT}(m) \to 0$ which leads to enhancement of high frequency noise. In addition, for those spatial frequencies for which $\mathrm{FFT}(m) = 0$, information cannot be obtained. (ii) Edge effects may give rise to spurious Fourier components. (iii) The numeric deconvolution in Eq. (6) is frustrated by a loss of information. These points are now considered in more detail.

3.1. The FFT(m) ≃ 0 problem

Concerning the first drawback of the FT-methods note that it follows from the work of Roth et al. [16] that:

$$j_x(k_x,k_y) \sim \mathrm{e}^{z\sqrt{k_x^2+k_y^2}}\, b_z(k_x,k_y z)$$

(a similar formula holds for j_y), which clearly implies an enhancement of noise of high spatial frequency k_x or k_y, in particular for a large distance of observation d, or equivalently for thick samples. They even state that for some filter functions there exist spatial frequencies for which $\mathrm{FFT}(m) = 0$ and where hence information cannot be obtained. They reduce the enhancement of high frequencies by using a cut-off filter. This leads to unnecessary loss of detail, while despite the filter often spurious 'fringes' arise at the edge of the sample (like those shown in Fig. 2h). Similar problems are encountered in other published FT methods. To illustrate this issues we show for a very thin sample ($t = 10^{-6}a$) in Fig. 3 $\mathrm{FFT}(m)$ for various ratios d/w, where w is the width of the sample (which for simplicity was taken as a square). Clearly, if $d/w = 1/256$ then $\mathrm{FFT}(m)$ is well above zero everywhere and the extreme values of $\mathrm{FFT}(m)$ differ by less than a factor 100. For $d/w = 10/256$ and larger, $\mathrm{FFT}(m)$ drops so quickly to zero for larger k-values that the numerical accuracy leads to noise around zero. For those combinations of d/w and k it leads to division by undetermined values (the noise) very close to zero and hence to extremely large high frequency components in the final g: this method breaks down completely for $d/w \geq 0.02$. Note that in the case of thick samples, since m contains an integral over the thickness, a small distance of observation is only realized close to the surface (the dependence of m on d and t takes this into account). One thus finds that only for small d and t, the $\mathrm{FFT}(m) \simeq 0$ problem is not important; for either thick samples or large observation distance this problem severely limits the use of FT-methods.

This is further illustrated by Fig. 2f–h which shows the results of model calculations, where a square wireframe with uniform current density is taken to generate the local field $H_z(i,j)$ and where the current is back-calculated from this H_z using the

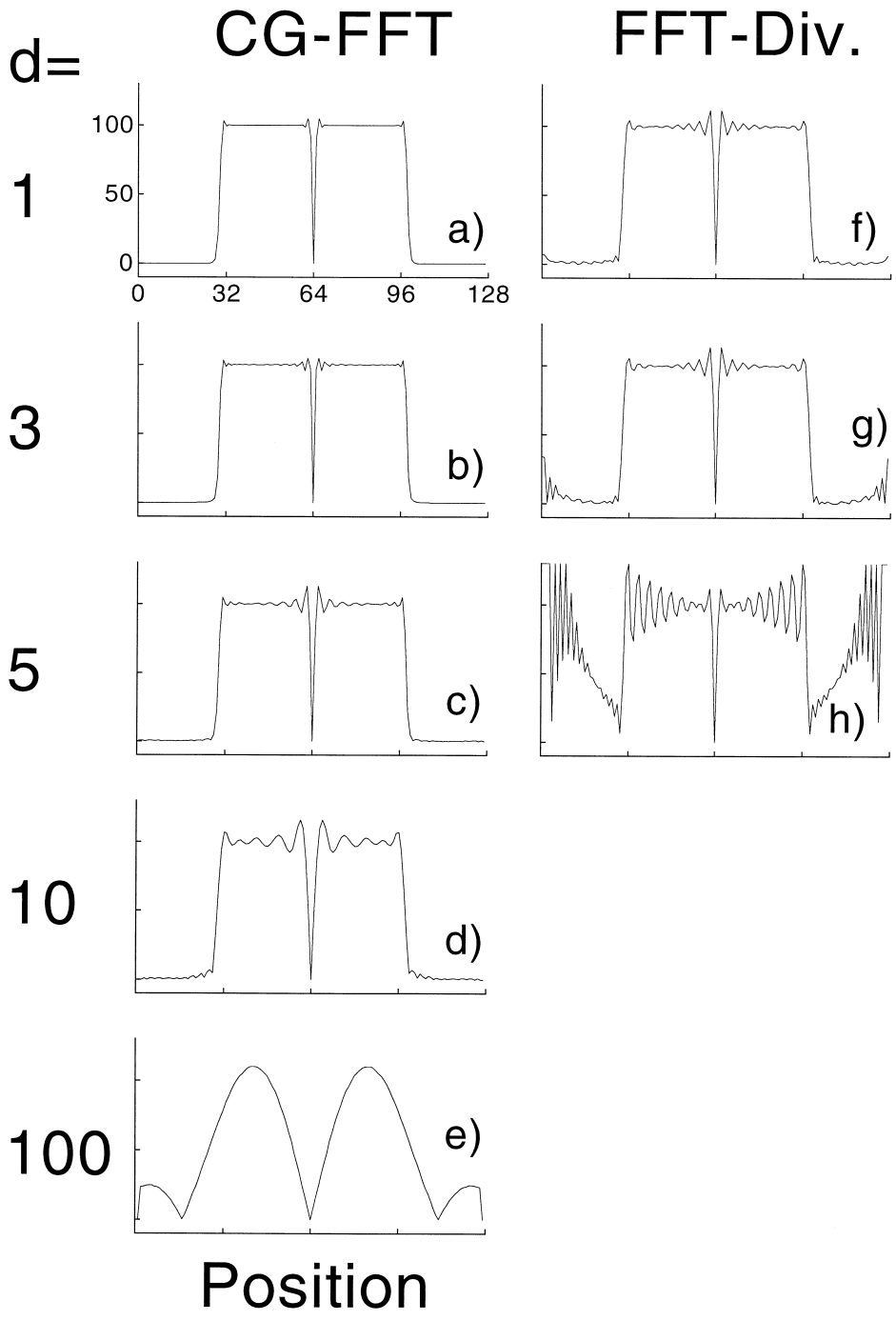

Fig. 2. Absolute value of the current as calculated from the new conjugate gradient with FFT matrix multiplication (CG-FFT) method and from division in the Fourier domain (FFT-Div.). The real current pattern is a square of size 68×68 centred at the origin with the current flow parallel to the x- and y-axes. Shown is the calculated absolute value of the current j along the x-axis, which is zero at the origin due to a sign change. Note that even up to the extremely large distance/width ratio $d/w = 100/128$ still reasonable values of the current are obtained by the CG-FFT method (a–e), while in the FFT-Div. method (f–h) intense oscillations inhibit calculations for $d/w > 5/128$.

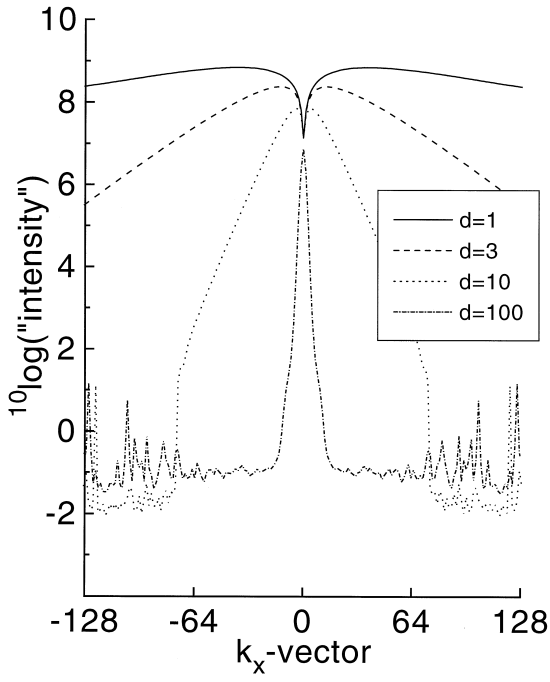

Fig. 3. Fourier transform of the matrix M. Since the matrix has circular symmetry, only the spatial frequency in the x-direction k_x (in units of $2\pi/256a$) is plotted along the horizontal axis. Vertically the ^{10}log of the absolute value of the scaled intensity is plotted, times the sign of the intensity. The intensity is scaled so that the ^{10}log of its absolute value is never negative. Plots are shown for various distances of observation d and for a fixed sample size of 256×256 (i.e. $w=256$). Clearly for large d ($d\geq10$) and equivalently also for large t, the Fourier-transform value is within calculational accuracy equal to zero for the larger k_x-values. This leads to large errors if the deconvolution is calculated by division in the Fourier domain.

method of Eq. (6), indicated in the figure by FFT-Div. For comparison in Fig. 2a–e results are shown from the new conjugate gradient method with FFT convolution (CG-FTT method) to be discussed below. The figure shows the absolute value of the current on a line through the centre of the sample. Note that in the centre of the sample the current changes sign and its value is zero. Clearly the oscillations at the sample edge for fixed d/w are larger for the FFT-Div. than for the CG-FFT method.

3.2. The edge problem

The second drawback, which applies for the numerical version of the FT-inversion only, is that the H_z data may not be zero at the edge of the H_z image. Consequently, the edges of the H_z-image show up in its Fourier transform and also in the calculated g-image. At large d/w or t/w the intensity of this spurious edge effect can completely wash out all information in the g-image.

3.3. The information loss problem

The third drawback of the FT-methods is that the deconvolution by Eq. (6) is frustrated by loss of information. In an experiment one tends to optimize the spatial resolution by having the sample occupy a large area of the H_z image. In particular for large d/w or t/w, the H_z-field will be significantly different from zero even far outside the H_z-image; hence some information is not measured. In more mathematical terms, the Greens function M in Eq. (4) is broad for large d/w or t/w and hence spreads the localized g over an area which may be significantly larger than the H_z-image. This problem is illustrated by the simple numerical example shown in Table 1. Note that in this example for simplicity the one-dimensional problem is considered. First consider the forward problem, corresponding to the calculation of H_z from a current flow pattern j. For this we need a convolution e.g. by matrix multiplication: $\boldsymbol{b}=\boldsymbol{M}\boldsymbol{g}$, which can be carried out directly using the full Toeplitz matrix, see line (a), or more efficiently, by the convolution of $\boldsymbol{g}$ with the generating vector $\boldsymbol{m}$ of $\boldsymbol{M}$ (cf. Eq. (5)):

$$(\boldsymbol{m}\otimes\boldsymbol{g})(i)=\sum_{j=\max(1,i+1-N)}^{\min(i,N)}\boldsymbol{g}(i)\boldsymbol{m}(i+1-j). \tag{7}$$

as illustrated in line (b). Note that the answer $\boldsymbol{b}$ is the middle part (underlined) of the direct convolution, this presents no problem: one just ignores the 'wings'. Now we consider the backward problem, corresponding to calculating the current flow pattern j, or equivalently g from H_z. For this we need a deconvolution. Solving $\boldsymbol{g}$ from Eq. (4) using deconvolution presents a problem since the wings are needed. If these are present the deconvolution is possible, see line (c) where $\ominus$ is used to indicate deconvolution. In our experiment, however, the wings are unknown since an image is measured of size $n\times n$, while the required current distribution has

Table 1
Numerical example to show the effects of convolution (indicated by $\otimes$) and deconvolution (indicated by $\ominus$). In (a) convolution by multiplication with the Toeplitz matrix M is shown, while in (b) the identical results of direct convolution or convolution by FFT are shown. Note that the same answer (underlined values) is found as in case (a). In (c) the result of deconvolution by FFT is shown to reproduce the value of g (underlined values) which was the input in (b). In (d) we show that loss of information, represented by zeroing the 'wings' of the vector $\boldsymbol{b}$ followed by a FFT deconvolution leads to erroneous results: the underlined values in (d) are clearly different from those in (c)

(a)	$\boldsymbol{Mg} = \boldsymbol{b}$	$\begin{pmatrix} 5 & 2 & 1 \\ 2 & 5 & 2 \\ 1 & 2 & 5 \end{pmatrix} \begin{pmatrix} 1 \\ 3 \\ 5 \end{pmatrix} = \begin{pmatrix} 16 \\ 27 \\ 32 \end{pmatrix}$
(b)	$(\boldsymbol{m} \otimes \boldsymbol{g}) = \boldsymbol{b}$	$(1\ 2\ 5\ 2\ 1) \otimes (1\ 3\ 5) = (1\ 5\ \underline{16}\ \underline{27}\ \underline{32}\ 13\ 5)$
(c)	$(\boldsymbol{b} \ominus \boldsymbol{m}) = \boldsymbol{g}$	$(1\ 5\ \underline{16}\ \underline{27}\ \underline{32}\ 13\ 5) \overset{\text{FFT}}{\ominus} (1\ 2\ 5\ 2\ 1\ 0\ 0) = (\underline{1}\ \underline{3}\ \underline{5}\ 0\ 0\ 0\ 0)$
(d)	$(\boldsymbol{b} \ominus \boldsymbol{m}) = \boldsymbol{g}$	$(0\ 0\ \underline{16}\ \underline{27}\ \underline{32}\ 0\ 0) \overset{\text{FFT}}{\ominus} (1\ 2\ 5\ 2\ 1\ 0\ 0) = (\underline{0.94}\ \underline{3.54}\ \underline{6.15}\ -3.38\ -0.013\ 1.10\ -1.52)$

also size $n \times n$. If one tries to pad up the measured image with zeros to be able to deconvolute it by IFFT, an erroneous answer is obtained as illustrated by line (d): the underlined values are clearly different from those in line (c). In practice, if the magnetic field H_z is measured over a region of space much larger than the sample, the error due to the zero-padding is not very large. However, since a detector with a fixed number of pixels is used, the use of such a wide field of view would lead to a significant loss of detail.

Clearly from the points discussed above FFT deconvolution is prone to problems. However, the three problems discussed above for deconvolution are absent for convolution: (i) convolution by FFT involves multiplication (and not division) of Fourier transforms so there is no potential problem from $\mathrm{FFT}(m) \simeq 0$ values; (ii) there is no edge problem since g is always zero outside the sample and (iii) there is also no information-loss problem because all information is in g which is known everywhere, while m may be also calculated everywhere. Hence, FFT methods can be used for high speed convolution. In fact, our new method, to be discussed below, makes use of this.

4. Direct methods

Now briefly some of the direct (i.e. non-FFT) methods are discussed. A first attempt to determine the currents in a disk-shaped sample from magneto-optical observations was made by Theuss et al. [6], who used adjustable currents through a set of concentric conducting rings to fit calculated H_z values to measured ones. Clearly, in this case the geometry of the current-pattern is fixed from the outset. This is a severe disadvantage e.g. for samples with unknown defects [18]. A method which finds not only the currents, but also the current flow pattern is given by Brandt [15]. Despite clever use of the physics involved, this method is not very efficient. Another method was later given by Xing et al. [19], which is also not very fast. In addition, both methods only work for infinitely thin samples and the obtained currents are hence very sensitive for the distance between sample and the H_z image. This problem was solved in our previous work [4], where a method is presented which handles samples of arbitrary thickness (this is the reason for integrating over the thickness in Eq. (3)). In addition, the required storage is reduced from $O(n^4)$ to $O(n^2)$ by employing the redundancy of information in the Toeplitz matrix M and the number of calculations is reduced from $O(n^6)$ to $O(n^{4.5})$. Regrettably, this is still much more than for the FT methods, where the number of calculations is $O(n^2 \ln n)$. We now present a new direct and exact method which has the same high speed as the FT methods, but without their drawbacks.

5. The new CG-FFT method

Our new method solves Eq. (4) using the iterative conjugate gradient method. The first estimate of the

solution $\boldsymbol{g}_1$ is made from Eq. (6) (note that this is the final answer in some of the other methods) which is a better starting value than previously proposed [4,19]. After initialization with the local gradient $\boldsymbol{p}_1 = \boldsymbol{q}_1 = H_z - \boldsymbol{M}\boldsymbol{g}_1$ at the starting value $\boldsymbol{g}_1$, the following steps [20] are iterated:

$$\begin{aligned} \boldsymbol{t}_i &= \boldsymbol{M}\boldsymbol{q}_i \\ \lambda_i &= \frac{\boldsymbol{p}_i \cdot \boldsymbol{q}_i}{\boldsymbol{q}_i \cdot \boldsymbol{t}_i} \\ \boldsymbol{g}_{i+1} &= \boldsymbol{g}_i + \lambda_i \boldsymbol{q}_i \\ \boldsymbol{p}_{i+1} &= \boldsymbol{p}_i - \lambda_i \boldsymbol{t}_i \\ \gamma_i &= \frac{\boldsymbol{p}_{i+1} \cdot \boldsymbol{p}_{i+1}}{\boldsymbol{p}_i \cdot \boldsymbol{p}_i} \\ \boldsymbol{q}_{i+1} &= \boldsymbol{p}_{i+1} + \gamma_i \boldsymbol{q}_i \end{aligned} \tag{8}$$

until the residue $\boldsymbol{q}_{i+1} \cdot \boldsymbol{q}_{i+1}$ is deemed sufficiently small. All these iteration steps require $O(n^2)$ operations, except the first one since the matrix $\boldsymbol{M}$ has n^4 elements. As discussed above, multiplication with the Toeplitz matrix $\boldsymbol{M}$ can be made without error as a convolution with its generating vector $\boldsymbol{m}$: the first equation is thus efficiently evaluated using FFT from $\boldsymbol{t} = \mathrm{IFFT}(\mathrm{FFT}(\boldsymbol{m}) \times \mathrm{FFT}(\boldsymbol{q}))$ in $O(n^2 \ln n)$ operations. This yields an enormous speed-up by a factor $n^2/\ln n$, which is the main improvement presented in this paper. Note that this convolution is again a linear (as opposed to circular) convolution.

The (I)FFT transforms are speeded up further by (i) calculating $\mathrm{FFT}(\boldsymbol{m})$ only once, by (ii) not performing the bit-shuffling operations of the FFT-algorithm [21], since these would be performed forward in the FFT and backward in the IFFT, of which the effects cancel since the product $\mathrm{FFT}(\boldsymbol{m}) \times \mathrm{FFT}(\boldsymbol{q})$ does not mix the elements of the transforms and by (iii) making use of the specific values of the factors $\sin \alpha/p$ and $\cos \alpha/p$ within the FFT algorithm for small integer p, which avoids multiplication in the first two stages of the FFT and the last two stages of the IFFT.

We should stress that our new method gives within numerical accuracy the same answer as the one presented in Ref. [4] (although the new method is much faster). In that paper the method is found to yield results consistent with bulk magnetometry. Also the results are proved to be insensitive for the distance of observation d provided that it is much smaller than the sample thickness t, typically $d < 0.1t$.

Timing results are presented in Fig. 4 which compares our previous method [4] with the new method just described. It is found that for the new method empirically $O(n^{2.8})$ operations are needed, which for the n-values used and taking into account the iterations needed agrees reasonably well with the value $O(n^2 \ln n)$ quoted above for one iteration step. As a consequence of using the FFT for the convolution zero padding is necessary: the FFT calculation (only) is done on matrices of size $2n \times 2n$. This implies a larger storage requirement and a $4\times$ larger number of operations. Due to this, the increase in speed with respect to our previous method [4] for 512×512 pixels is found to be a factor 135. Inci-

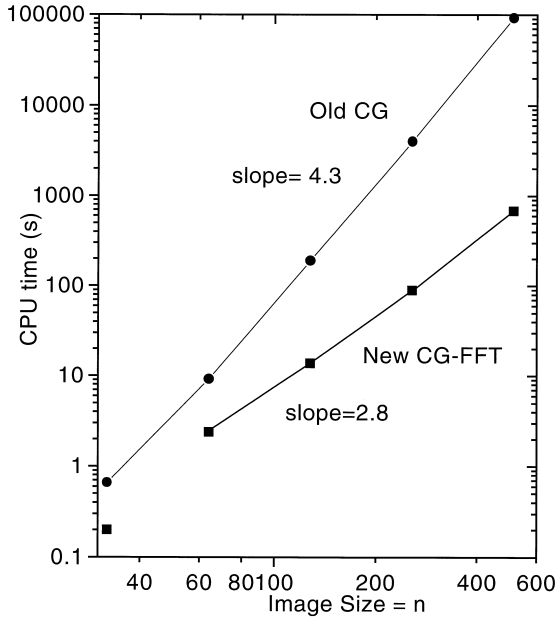

Fig. 4. CPU time on a single RS6000/58H processor for the standard conjugate gradient (CG)-algorithm [4] and for the new conjugate gradient with fast Fourier transform matrix multiplication (CG-FFT) method. Note the increase in speed by a factor 135 at linear size $n = 512$.

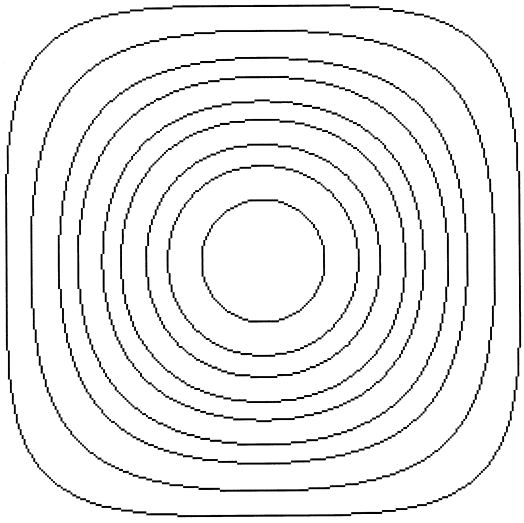

Fig. 5. Flow lines of the current as calculated from the H_z-field for the extremely large distance/width ratio $d/w = 100/128$ using the new CG-FFT method. The current flow which was used to generate the H_z-field would correspond to equally spaced 'concentric' squares. For the absolute value of the current see Fig. 2e.

dentally, this is much smaller than $512^{(4.5-2.8)}$ due to a larger prefactor to the $O(n^{2.8})$ behaviour than to the $O(n^{4.5})$ behaviour. The most time consuming step in the present algorithm is the FFT, which can be easily programmed for parallel computing thus leading to much faster calculation, possibly even to real-time calculation (i.e. at video speed). As shown in Fig. 2 the CG-FFT method is stable at least up to $d/w = 100/128$. For that large distance the profile of the current (subfigure e) has lost much of its detail. However, as shown in Fig. 5, the current flow lines are still reproduced reasonably well (the correct flowlines would have been equidistant 'concentric' squares).

It turns out that for small d the addition of random noise to the image has hardly any influence on the speed of convergence and hence on the time needed for the calculations. Of course, the addition of noise to H_z generates noise in the calculated currents. This noise is well-behaved and does not lead to large oscillations, e.g. at the edge. For large d there may not exist a current pattern which can reproduce a noisy H_z-image. This is because at large d the H_z image is always 'smooth' since it is the convolution of the current pattern defining g and the matrix m, which is a broad peak for large d.

6. Conclusion

We have presented a very efficient inversion scheme to find the 2D current pattern from its associated magnetic field. The number of operations needed for this method is of the same order as for the published FFT methods, but it avoids the drawbacks which are inherent to using Fourier transform solutions for this problem. The resulting answer is rigorously correct and no smoothing or filtering is necessary. This method may lead in the near future to real-time applications (the result from the previous inversion may be used as initialization for the next one). Furthermore, it opens a path to large scale simulations of current flow in non-linear conductors (such as superconductors) as pioneered by Brandt [10] since the slowest step in that procedure is the same inversion, of Eq. (4), which is the subject of the present work.

Acknowledgements

We thank G. Doornbos for discussions on the Conjugate Gradient Algorithm. This work is part of the research program of the Stichting Fundamenteel Onderzoek der Materie (FOM), which is financially supported by the Nederlandse Organisatie voor Wetenschappelijk Onderzoek (NWO).

References

[1] D.S. Barth, W. Sutherling, J. Engel, J. Beatty, Science 223 (1984) 293.
[2] B.J. Roth, J.P. Wikswo, Biophys. J. 48 (1985) 93.
[3] J.P. Wikswo, B.J. Roth, Electroencephalogr. Clin. Neuro. 69 (1988) 266.
[4] R.J. Wijngaarden, H.J.W. Spoelder, R. Surdeanu, R. Griessen, Phys. Rev. B 54 (1996) 6742.
[5] A.E. Pashitski, A. Gurevich, A.A. Polyanskii, D.C. Larbalestier, A. Goyal, E.D. Specht, D.M. Kroeger, J.A. DeLuca, J.E. Tkaczyk, Science 275 (1997) 367.
[6] H. Theuss, A. Forkl, H. Kronmüller, Physica C 190 (1992) 345.
[7] M.R. Koblischka, R.J. Wijngaarden, Superconduct. Sci. Technol. 8 (1995) 199, and references therein.

[8] E.H. Brandt, M.V. Indenbom, A. Forkl, Europhys. Lett. 22 (1993) 735.
[9] E.H. Brandt, Physica C 235–240 (1994) 2939.
[10] E.H. Brandt, Phys. Rev. Lett. 74 (1995) 3025.
[11] D.J. Frankel, J. Appl. Phys. 50 (1979) 5402.
[12] E. Zeldov, J.R. Clem, M. McElfresh, M. Darwin, Phys. Rev. B 49 (1994) 9802.
[13] Yu.A. Fedorov, V.G. Fleisher, M.G. Semenchenko, Physica C 217 (1993) 63.
[14] J.D. Jackson, Classical Electrodynamics, 2nd ed., Wiley, New York, 1975, Eq. 5.14.
[15] E.H. Brandt, Phys. Rev. B 46 (1992) 8628.
[16] B.J. Roth, N.G. Sepulveda, J.P. Wikswo, J. Appl. Phys. 65 (1989) 361.
[17] T.H. Johansen, M. Baziljevich, H. Bratsberg, Y. Galperin, P.E. Lindelof, Y. Shen, P. Vase, Phys. Rev. B 54 (1996) 16264.
[18] M.R. Koblischka, R.J. Wijngaarden, D.G. de Groot, R. Griessen, A.A. Menovsky, T.W. Li, Physica C 249 (1995) 339.
[19] W. Xing, B. Heinrich, H. Zhou, A.A. Fife, A.R. Cragg, J. Appl. Phys. 76 (1994) 4244.
[20] M. Hestenes, Conjugate Direction Methods in Optimization, Springer, New York, 1980.
[21] W.H. Press, B.P. Flannery, S.A. Teukolski, W.T. Vetterling, Numerical Recipes, Cambridge University Press, Cambridge, 1989.